LOADING-RATE DEPENDENCE OF MODE I FRACTURE BEHAVIOR OF RUBBER-TOUGHENED PMMA

M. Todo and K. Takahashi

Research Institute for Applied Mechanics, Kyushu University, Kasuga, Fukuoka 816-8580, Japan

ABSTRACT

Mode I fracture tests of three kinds of rubber-toughened PMMA (RT-PMMA) and a neat PMMA were performed at different loading rates using three testing systems, namely, a servohydraulic testing machine, an instrumented drop weight impact tester and a modified SHPB impact test system. The critical mode I energy release rates, G_{Ic}, were evaluated at the different loading rates and the loading-rate dependences of the G_{Ic} values were examined. Two of the RT-PMMA's exhibited that their G_{Ic} values increased with increase of loading-rate; on the other hand, the G_{Ic} of the other RT-PMMA tended to decrease at the loading-rates higher than 1 m/s. Effects of loading-rate on the damage zones generated in the vicinity of crack-tips were also investigated by optical microscopy. The rate dependence of the G_{Ic} values was then correlated with that of the damage zone formation in terms of energy dissipation process.

KEYWORDS

Rubber toughening, Mode I crack propagation, Toughening mechanisms, Impact testing, Craze formation

INTRODUCTION

To increase the impact resistance of a transparent thermoplastic PMMA, different types of rubber-toughened PMMA (RT-PMMA) have been developed by blending rubbery phases with PMMA matrices, and attempts made to characterize their mechanical properties. The effects of loading-rate on the fracture behavior of RT-PMMA and neat PMMA have been investigated [1-3]. Todo et al. [3] performed mode I fracture tests of two types of RT-PMMA at loading rates from 10^{-4} to 13m/s using a modified servohydraulic testing machine. They found that the maximum mode I stress intensity factor, K_{Imax}, and the maximum mode I energy release rate, G_{Imax}, of one of the RT-PMMA's containing 20wt% rubber particles suddenly decreased at the rates higher than 1 m/s, while the other containing 40wt% rubber particles didn't exhibit such rate dependence. Some attempts have also been made to characterize the deformation and fracture behavior of RT-PMMA from microscopic points of view [4-7]. Todo et al. [7], for example, showed that the toughening mechanism of RT-PMMA is closely related to the microdamage formations such as microcrazing and matrix shear deformation generated in the vicinity of crack-tip.

The aim of the present study is to characterize the effects of loading-rate on the mode I fracture behavior of three types of RT-PMMA by correlating two different aspects, that is, macroscopic fracture property such as the critical mode I energy release rate, G_{Ic}, and microscopic damage formation in the vicinity of crack-tip. To evaluate their G_{Ic} values, mode I fracture tests were performed at different loading-rates from 10^{-5} to 9m/s

using three kinds of testing system. Damage zones developed during crack propagation were also observed using an optical microscope to examine the rate effects on the damage zone formation. A simple model to explain one of the rate dependences observed was then proposed on the basis of the energy dissipation mechanism during crack propagation.

EXPERIMENTAL

Material and Specimen

Three kinds of RT-PMMA were studied: press formed containing 8 wt% butadiene rubber (PM8), extruded containing 20wt% butyl acrylate-co-styrene rubber (EM20) and press formed containing 40wt% butyl acrylate-co-styrene rubber (PM40). A neat PMMA made by cast (CU) was also examined for comparison.

Single edge notch bending (SENB) specimens were prepared for mode I fracture testing. The length L, width W, thickness B and the initial notch length a were 80-90mm, 15mm, 5mm and 7.5mm, respectively. For each specimen, a pre-crack was carefully introduced by drawing a new razor blade along the tip of the machined notch.

Mode I Fracture Testing

Three-point bending fracture tests at low displacement rates from 10^{-5} to 10^{-2}m/s were conducted using a servohydraulic testing machine. The span length was 40mm. Load-time and displacement-time relations were recorded on a digital recorder. The critical mode I energy release rate, G_{Ic}, can be evaluated using the following formula [8]:

$$G_{Ic} = \frac{U}{BWf} \tag{1}$$

where f is the energy calibration factor given as a function of a/W. For each specimen, the critical strain energy U was calculated by integrating the area under its load-displacement curve up to a critical point defined as the point at which the stiffness of the specimen suddenly decreased as a result of the initiation of crack propagation. An example of the SENB test data is shown in Figure 1. It is noted that for the neat PMMA, the critical load was found to be equivalent to the maximum load.

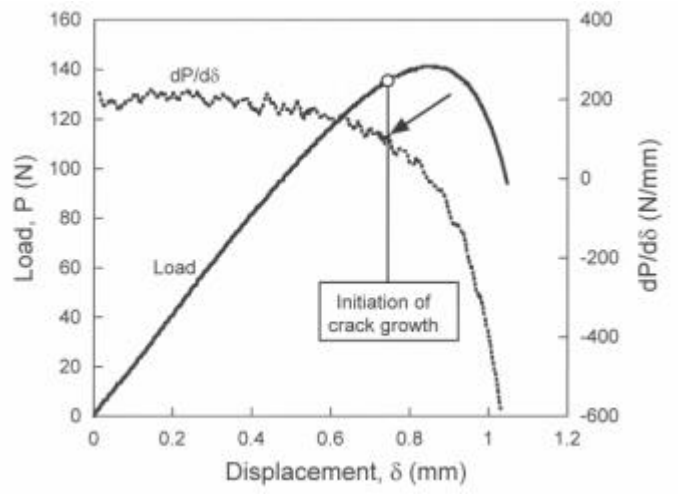

Figure 1: An example of SENB test results. The arrow indicates the initiation of crack growth.

An instrumented drop weight impact test system was used for the fracture tests at the loading rates from 0.5 to 1.6m/s. Displacements at the loading points were measured using an optical displacement measuring device [9]. An example of the test data is shown in Figure 2(a). It is seen that the peaks of the crack-tip strain and the load took place at the same time. It is therefore presumed that the maximum loads were equivalent to the critical loads in this series of impact test. The G_{Ic} values were then evaluated using the same procedure

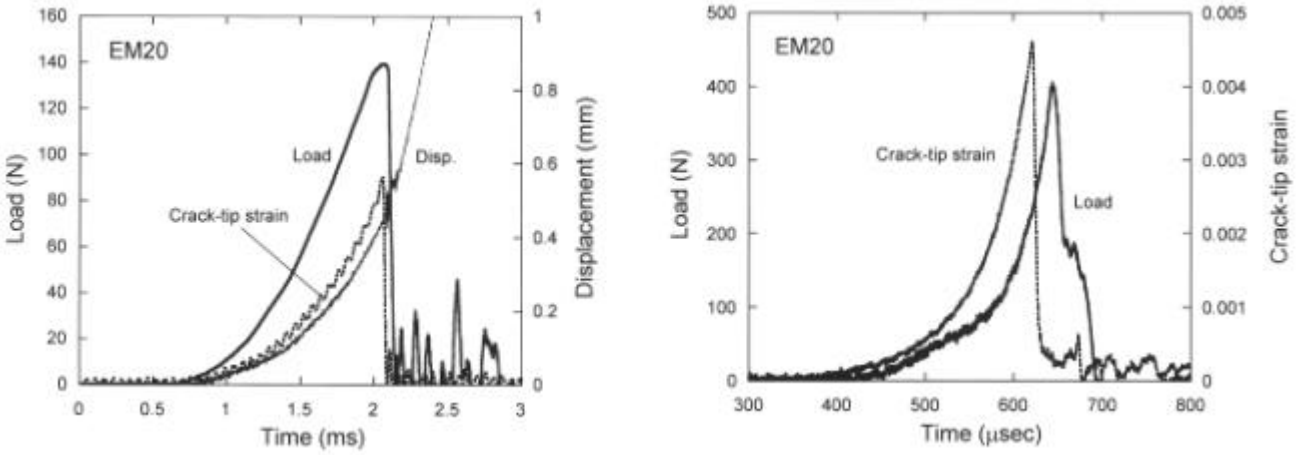

(a) Drop weight impact test (b) SHPB impact test

Figure 2: Examples of impact fracture test data.

as used for the low-rate testing.

Impact fracture tests at the loading rates from 5 to 9m/s were carried out using a SHPB impact bending test system[10]. The SHPB system is shown in Figure 3. For each specimen, strain in the vicinity of the crack-tip was measured to determine the initiation of crack growth. In the present study, to reduce dynamic effects, silicon rubber sheet 1.5mm thick was placed between the striker and the input bar as shown in Figure 3. An example of the test data is shown in Figure 2(b). The load is the sum of the bads measured from the output bars. It appears that dynamic bending effects were dramatically reduced since the initiation of the load was almost identical with that of the crack-tip strain, suggesting the contact between the specimen and the output bars in the initial stage of the loading. It was therefore presumed that the static procedure of G_{Ic} evaluation described above was applicable to the present SHPB test results.

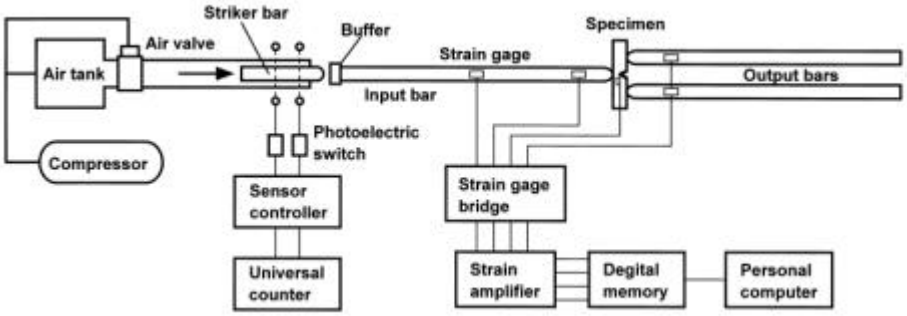

Figure 3: SHPB impact bending test system.

Damage zones generated in the vicinity of crack-tips during crack propagation were observed using an optical microscope. Rectangular sections containing propagating cracks were prepared from the tested specimens at different loading rates. Their surfaces were polished and then observed using the microscope.

RESULTS AND DISCUSSION

Rate Dependence of Critical Mode I Energy Release Rate

The G_{Ic} values obtained are shown as functions of loading rate in Figure 4. The G_{Ic} of CU increased with increase of loading rate up to 10^{-2}m/s and became constant up to 1m/s and then slightly decreased at the higher rates. The G_{Ic} of EM20 was almost independent of loading rate up to 1m/s and then decreased at the higher rates. On the other hand, PM8 and PM40 exhibited similar rate dependences. Their G_{Ic} values were almost independent of loading rate up to 10^{-1}m/s and then increased with increase of loading rate. It is noted that the G_{Ic} of PM8 was the highest of all the materials at every loading rates although PM8 only contains

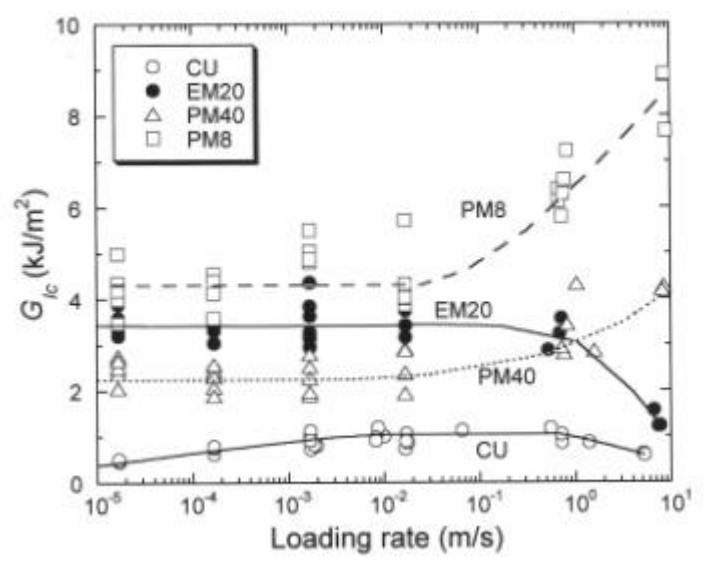

Figure 4: Dependence of loading rate on G_{Ic}.

8wt% rubber particles. It is thus understood that higher toughness can be achieved by blending butadiene rubber even in a relatively low rubber content.

Damage Zone Observation

A propagating crack in CU at a low loading rate and the damage zones developed in PM8 and EM20 at a low and an impact rate are shown in Figure 5 and Figure 6, respectively. It is observed from Figure 5 that there was no damage zone formed in CU. On the other hand, cloud-like damage zones were developed during crack propagation in the RT-PMMA's. It has been known that a collection of microcrazes generated in the surroundings of rubber particles forms a damage zone in the vicinity of a crack-tip [7]. It is noted that PM8 possessing the highest G_{Ic} showed the largest damage zone among the three RT-PMMA's. It has been recognized that the additional energy dissipation due to damage zone formation results in the toughening of RT-PMMA [7]. Thus, larger damage zone corresponds to higher G_{Ic} value. At the high rate, the damage zones of EM20 became very thin, while PM8 still exhibited an extensive damage zone even at the high rate. It is understood that for all the RT-PMMA's, the size of damage zone decreased with increase of loading rate.

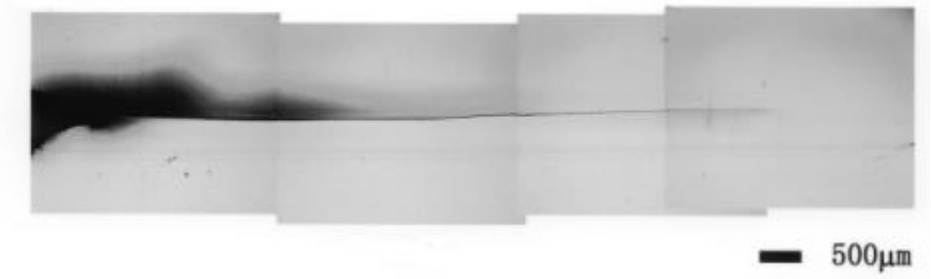

Figure 5: Propagating crack in CU at a low rate.

Mechanism of Rate Dependence of EM20

A crack growth behavior in a RT-PMMA under a steady-state condition is considered to understand the peculiar rate effect observed for EM20. It is assumed that the G_{Ic} of the RT-PMMA can be expressed as [11]:

$$G_{Ic} = G_{Damage} + G_{Surface} \tag{2}$$

where G_{Damage} and $G_{Surface}$ are the contributions of damage zone formation and surface energy to G_{Ic}. It is also assumed that G_{Damage} can be simply approximated by

$$G_{Damage} = w\ddot{O} \tag{3}$$

where w is the energy required to create a unit amount of microcraze and $\boldsymbol{F}$ is the total amount of microcrazes generated in a damage zone during the crack growth. If $G_{Surface}$ is negligibly small compared to G_{Damage}, then Eqns 2 and 3 give

$$G_{Ic} = G_{Damage} = w\ddot{O} \tag{4}$$

The results shown in Figure 6 suggest that $\boldsymbol{F}$ can be expressed as a function of loading rate such that $\boldsymbol{F}$ decreases as loading rate increases as shown in Figure 7. If w is assumed to be expressed as a function of loading rate such that w increases as loading rate increases as shown in Figure 7, then G_{Damage} exhibits a loading rate dependence shown in Figure 7 that is similar to the rate dependence of the G_{Ic} of EM20 shown in Figure 4. Thus, the rate effect on the G_{Ic} of RT-PMMA may be elucidated by correlating the energy dissipation process with microdamage formation during crack growth.

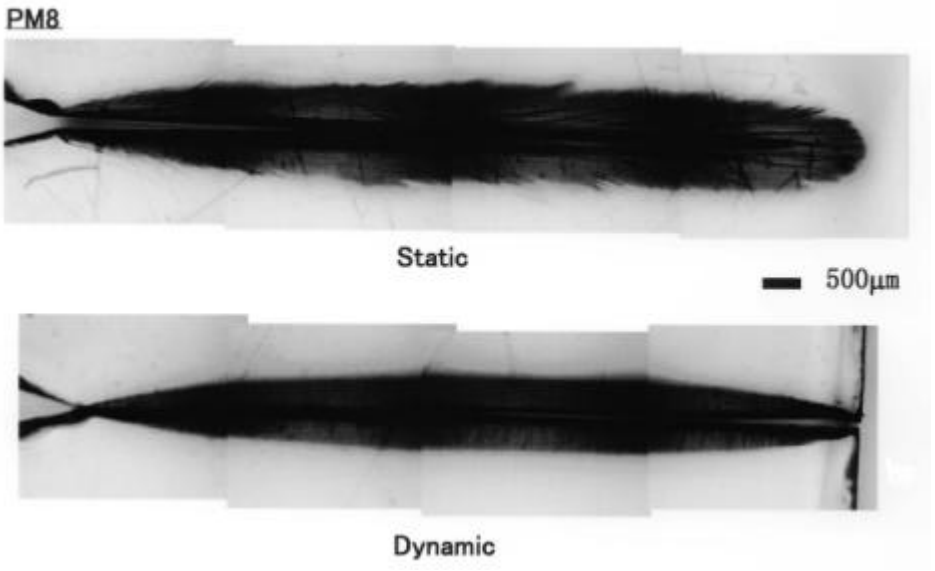

(a) PM8 at a low and an impact rate

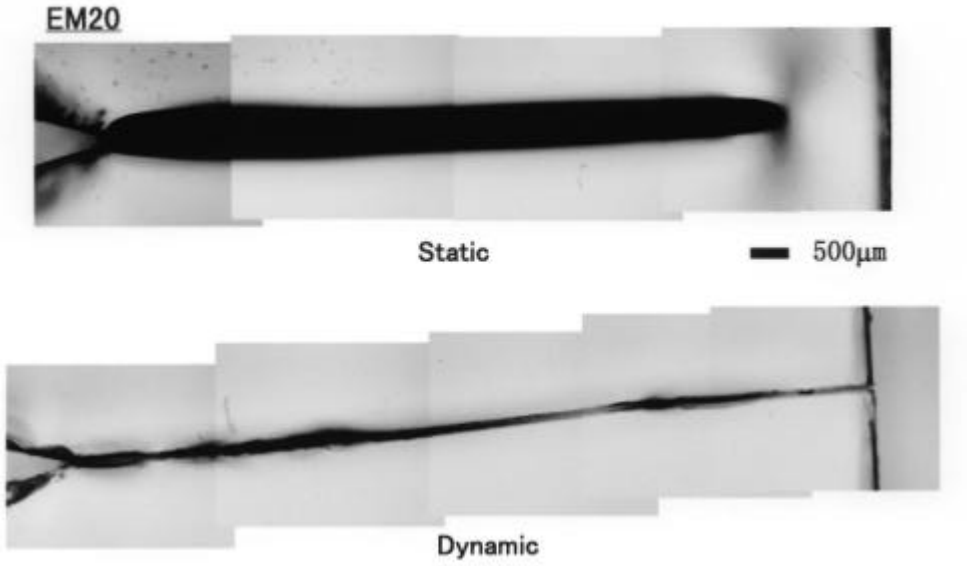

(b) EM20 at a low and an impact rate

Figure 6: Damage zone formation in RT-PMMA.

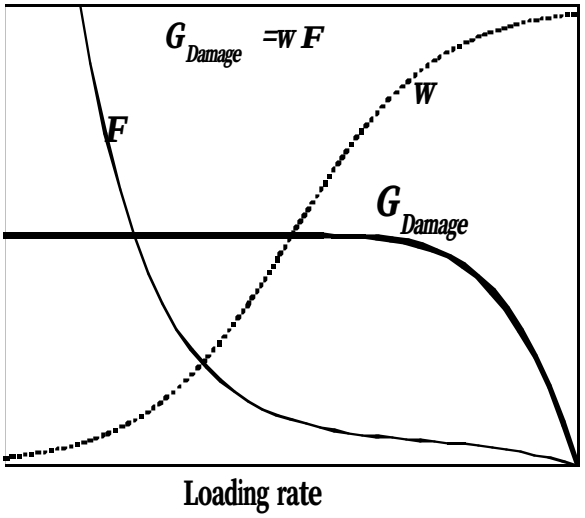

Figure 7: A mechanism of the loading rate dependence of EM20.

CONCLUSIONS

Loading-rate dependences of the critical mode I energy release rates G_{Ic} of three different RT-PMMA and a neat PMMA were investigated in a range of loading rate using three different testing systems. The following conclusions were reached:

(1) The G_{Ic} of CU increased with increase of loading rate up to 10^{-2}m/s and became constant up to 1m/s and then slightly decreased at the higher rates. The G_{Ic} of EM20 was almost independent of loading rate up to 1m/s and then decreased at the higher rates. The G_{Ic} values of PM8 and PM40 were almost independent of loading rate up to 10^{-1}m/s and then increased with increase of loading rate. PM8 exhibited the highest G_{Ic} at every loading rates.

(2) Cloud-like damage zones were developed during crack propagation in the three RT-PMMA's. PM8 showed the largest damage zone corresponding to the highest G_{Ic}. For all the RT-PMMA's, the size of damage zone decreased with increase of loading rate.

(3) The loading rate dependence of the G_{Ic} of RT-PMMA may be correlated with the rate dependence of damage zone formation in terms of the energy dissipation mechanism due to microdamage formation.

REFERENCES

1. Beguelin, Ph., and Kausch, H.H. (1994) *J. Mater. Sci.* 29, 91.
2. Beguelin, Ph., Julien, O., Monnerie, L. and Kausch, H.H. (1994) *Proc. the American Chemical Society Division of Polymeric Materials: Science and Engineering* 70, 147.
3. Todo, M., Takahashi, K., Beguelin, Ph. and Kausch, H.H. (1999) *JSME Inter. Journal (A)* 42, 49.
4. Lovell, P.A., Ryan, A.J., Sherratt, M.N. and Young, R.J. (1994) *Proc. 9th Inter. Conf. on Deformation, Yield and Fracture of Polymers,* 3/1.
5. Plummer, C.J.G., Beguelin, Ph. and Kausch, H.H. (1996) *Polymer* 37, 7.
6. Kausch, H.H., Beguelin, Ph., Lu, A., Plummer, C., Fond, C. and Schirrer, R. (1997) *Proc. 9th Inter, Conf. on Fracture* 6, 2835.
7. Todo, M., Takahashi, K., Jar, P.-Y.B. and Beguelin, Ph. (1999) *JSME Inter. Journal (A)* 42, 585.
8. ASTM D 5045-91a: Standard Test Methods for Plane-Strain Fracture Toughness and Strain Energy Release Rate of Plastic Materials.
9. Todo, M., Nakamura, T., Mada, T. and Takahashi, K. (1998) *Advanced Comp. Mater.* 7, 285.
10. Todo, M. and Takahashi, K. (1999) *Proc. the ASC 14th Tech. Conf.,* 131.
11. Tohdoh, M., Chaturvedi, S.K. and Sierakowski, R.L. (1996) *Inter. J. Fracture* 75, 285.